船舶技術研究所報告　第30巻　第6号　研究報告（平成5年11月）

Experimental Study on Spray Shape, Spray Drag and Flow Field of Surface-Piercing Vertical Strut Advancing at High Speed*

By
Takeshi FUWA**, Nobuyuki HIRATA**
Toshifumi HORI**, Jun-ichi FUJISAWA**

Abstract

In order to understand the nature and flow structure of the spray, some experiments of strut with circular arc cross section are performed in a towing tank. Measurement of the spray is not so easy as that of flow field around a ship model because of its delicate and unsteady nature. As touch sensors are not applicable for the measurement of spray, an image processing technique using LASER is applied in the present study. The shape of the spray and the velocity on the spray surface are measured as well as the wave height in the near field of the strut. Based on the measurement of mass flux and impulsive pressure of the spray distributed in a vertical cross section behind the strut, a spray drag due to the momentum loss is estimated and discussed. Results of some theoretical calculations are compared with the measurements.

Nomenclature

c :	Chord length of strut	(m)
B :	Breadth of strut	(m)
d :	Draught of strut	(m)
S :	Wetted area of strut in still water	(m^2)
∇ :	Displacement	(m^3)
t :	Time	(sec)

* Similar contents to this paper were presented at HPV'92-CHINA Conference [1], and some additional experimental data and further investigations are made for a frictional drag and a turbulence stimulator.

** Ship Performance Division

Received on July 12, 1993
Accepted on September 8, 1993

X, Y, Z :	Fixed coordinate system of strut	(m)
x, y, z :	Non-dimensional fixed coordinate system of strut, $x=X/c,\ y=Y/c,\ z=Z/c$	
$\boldsymbol{e}_x, \boldsymbol{e}_y, \boldsymbol{e}_z$:	Fundamental unit vector	
V :	Speed of strut	(m/sec)
ν :	Kinematic viscosity of water	(m^2/sec)
ρ :	Density of water	(kg/m^3)
F_n :	Froude number, $V/\sqrt{gc}$	
R_n :	Reynolds number, $V\,c/\nu$	
x_{tr} :	Point of transition from fore end	
R_{tr} :	Reynolds number at the point of transition, $V\,x_{tr}/\nu$	
D :	Drag	(N)
C_D :	Drag coefficient, $D/\frac{1}{2}\rho V^2 S$	
D_{SPRAY} :	Spray drag	(N)
C_T :	Total drag coefficient	
C_V :	Total viscous drag coefficient	
C_{F_0} :	Frictional drag of plate	
C_F :	Frictional drag coefficient of strut	
C_W :	Wave-making drag coefficient	
C_{WP} :	Wave pattern drag coefficient by wave analysis	
C_{SPRAY} :	Spray drag coefficient	
$C_{PROFILE}$:	Profile drag coefficient	
C_{TIP} :	Tip drag coefficient	
C_{RES} :	Generalized residuary drag coefficient, $C_T-C_{PROFILE}-C_W-C_{SPRAY}$	
C_{TWS} :	Total drag coeffcient with Hama's patch	
ΔC_{FTL} :	Difference of frictional drag coefficient between turbulent and laminar, $C_{F_0}(turb)-C_{F_0}(lam)$	
ΔC_F :	Frictional drag coefficient of increasing wetted area by spray/disturbed free surface	
α :	Air drag factor	(kg/sec)
k :	Three dimensional form factor based upon flat plate friction	
m :	Mass of water particle	(kg)
g :	Gravitational constant	(m/sec^2)
$\boldsymbol{r}$:	Position vector of water particle	
m^* :	Mass flux rate of total spray	(kg/sec)
Q^* :	Flux rate of water in weight, m^*g	(kg • m/sec^3)
P^* :	Impulsive force of total spray	(N)
X_0, Y_0, Z_0 :	Initial position of water particle	(m)
V_0 :	Initial velocity of water particle	(m/sec)
F_{n0} :	Froude number based on V_0, $V_0/\sqrt{gc}$	
l_{ts} :	Length of Hama's patch	(m)
H_W :	Wave height	(m)

List of Contents

Page

Abstract 1
Nomenclature 1
1. INTRODUCTION 3
2. EXPERIMENT 4
2.1 Models of Strut 4
2.2 Resistance Test and Wave Measurement 7
2.3 Measurements of Spray Shape and Velocity 7
2.4 Measurements of Mass Flux and Impulsive Pressure of Spray behind Strut 8
2.5 Turbulence Stimulation and Frictional Drag 10
3. RESULTS AND DISCUSSION 11
3.1 Resistance Test Results and Overall Characteristics of Flow Field 11
3.2 Spray Shape and Velocity 15
3.3 Mass and Momentum Flux of Spray 19
3.4 Drag Components 20
3.4.1 Separation of drag components 20
3.4.2 Wave-making drag and viscous drag 21
3.4.3 Estimation of state of boundary layer and turbulence stimulator 24
3.4.4 Spray drag 26
3.4.5 Total drag and drag composition 27
4. CONCLUSIONS 30
Acknowledgement 30
References 30

1. INTRODUCTION

Various kinds of proposals, research and developments on new-type high-speed ships have been seen in the recent worldwide trend of development of high performance ships. One of the most ambitious and remarkable ones is *the Techno-Superliner Project* of Japan. The target of the project is to design and construct a large high speed cargo ship which has 1,000 tons pay load, 50 knots service speed and 500 nautical miles endurance.

Surface-piercing struts are used for some new type high speed vessels such as *TSL-F* (foilborne type *Techno-Superliner*), and spray phenomena draw attention of the ship designers again. When a surface-piercing strut runs at high speed, the spray phenomena are observed. Though the phenomena have not yet been defined strictly, they are generaly considered as follows; a thin water film creeps up the side of the strut, separates from the surface and flies away as water particles. A considerable amount of drag seems to be caused by the spray.

Comprehensive studies on the hydrodynamic characteristics of the surface-piercing strut were carried out in the early stage of the development of hydrofoil or SWATH ship. Some experimental data on the drag, spray, ventilation etc. were obtained and utilized for the ship design [2-5]. At present empirical formula for the spray drag and some practical data are available [2-4]. There are studies on some devices such as spray rails to reduce the spray and spray drag [3,6,7]. Few study on the nature of the spray, however, is known and theoretical modelling of the spray has not yet been established. Therefore the techniques of the computational fluid dynamics (CFD) are not applied to the flow field with the spray phenomena, even though the recent progress in computer science and CFD is remarkable and they are also applied to the flow analysis of high-speed ships. The modelling of the spray is keenly expected.

The spray phenomena are specific for a relatively high speed flow. The water wave theory and free stream model are applied to investigate the spray, but some more fundamental studies are necessary to clarify the inception condition, mechanism and the hydrodynamic definition of the spray. The governing equations for the whole flow field and their solutions should be studied on the basis of the results and the modelling of the spray.

The present study is defined as an extension of a hydrodynamic study on the same strut model [5] into the higher speed region. Special attention is focused on the spray structure and the spray drag.

2. EXPERIMENT

Measurements are carried out in the Mitaka No.3 Ship Model Experimental Tank ($Length \times Breadth \times Water\ depth = 150m \times 7.5m \times 3.5m$) of the Ship Research Institute for several times. Fig. 1 outlines the arrangement for the measurements in the towing tank. The items of measurement are total drag, wetted area, wave pattern, thin water film on strut, spray shape, velocity on spray surface, mass flux of spray, and impulsive pressure of spray.

2.1 Models of Strut

Two geometrically similar vertical strut models with circular arc cross section are prepared for the tank experiments. The chord length of the models are $0.8m$ and $0.3m$. In Table 1 the principal particulars of the models are shown. Fig. 2 shows the shape and size of the larger strut, and

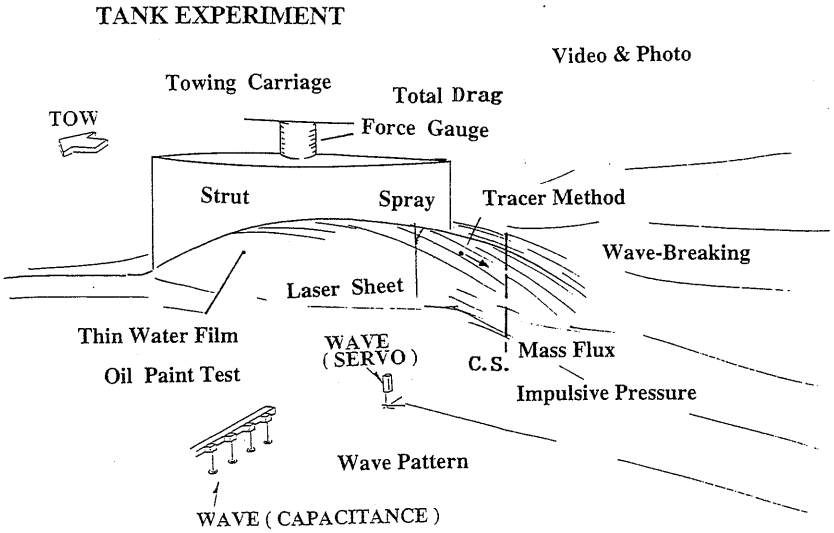

Fig. 1 Arrangement of Experiment

Table 1 Principal Particulars of Strut Models

Item	Symbol (Unit)	Larger Strut	Smaller Strut
Chord Length	c (*m*)	0.80	0.30
Breadth	B (*m*)	0.12	0.045
Depth	(*m*)	1.60	0.60
Standard Draught	d (*m*)	1.20	0.45
Displacement	▽ (m^3)	0.643	0.0034
Wetted Surface Area	S (m^2)	1.93	0.271
Cross Section		Double Arc	
Thickness Ratio	B/c	0.15	
Aspect Ratio	d/c	1.5	

coordinate system. The larger model mainly is used in the experiments.

Photo 1 shows the turbulence stimulator used in the experiments. They are so-called Hama's Patch recommended for the tank test of high speed crafts in the Report of 19th ITTC [8]. They are hand-made, layered vinyl tape and are applied only for the larger strut. The size, shape and position of the turbulence stimulator are shown in Fig. 2 as well.

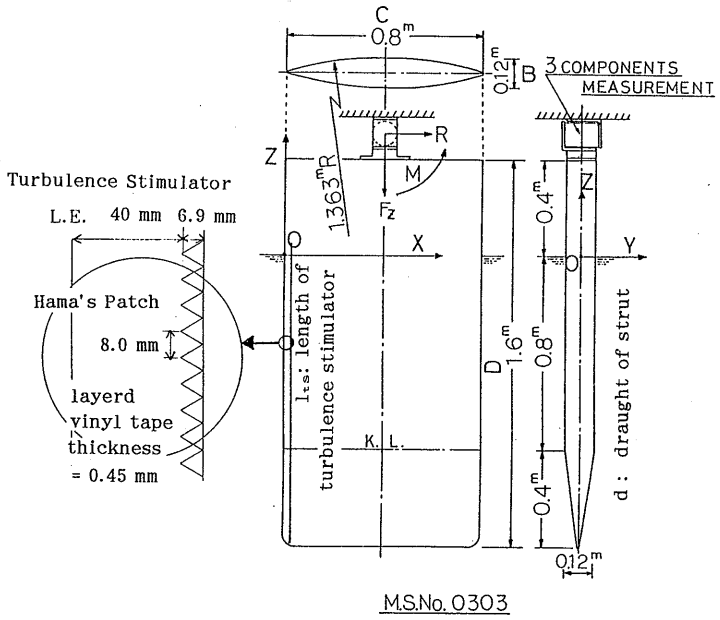

Fig. 2 Strut Model, Coordinate System & Turbulence Stimulator

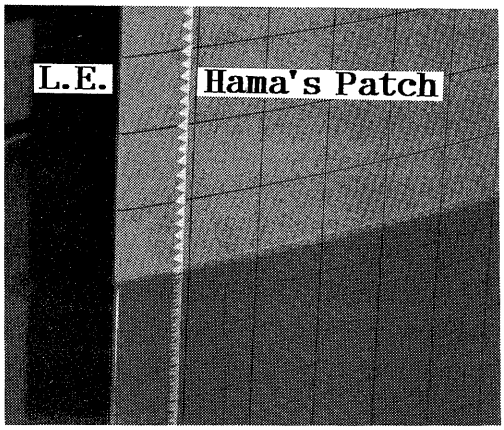

Photo 1 Hama's Patch on Surface-Piercing Strut

2.2 Resistance Test and Wave Measurement

The resistance tests are performed in a fixed dipping and trim condition. In order to measure a total drag, a 3-component force gauge is equipped to the model as shown in Fig. 2. Because of the restriction of the carriage speed and the capacity of available force gauges, the smaller model is used for the test in the higher speed region.

At first, no kinds of turbulence stimulators are applied and the leading edge part of the strut is kept smooth, because the objective is the measurement of the spray. In order to get rid of an uncertainty in the estimation of a frictional drag component due to the transition of a boundary layer, experiments with turbulence stimulator are also performed.

For the wave records in the far field from the strut, a capacitance type probe located in the middle of the tank is used. For the measurement of wave pattern in the near field, a servo-mechanism type probe mounted on a traversing mechanism is used. For the measurement of the thin water film creeping up on the strut surface, the same servo-mechanism type probe and a rotary scanning device with a potentiometer is applied. For the measurement of the wetted surface area, an oil paint method is applied and compared with the photographic and video records.

2.3 Measurements of Spray Shape and Velocity

Measurements of the shape and location of the spray are rather difficult by the ordinary sensors [9, 10]. Flow visualization and image data processing techniques are applied [11]. The surfaces of wave and spray are visualized by means of a sheet ray projected from a cylindrical collimator and an Argon LASER system. Because the shape of the spray surfaces is not simple in its topology, sometimes two cameras are necessary to cover the whole range of view from fixed positions. Image data recorded by video cameras are calibrated and analysed by a standard method. An explanation of the flow visualization by a LASER sheet and image data processing system is shown in Fig. 3.

In order to measure the flow velocity on the spray surface, a tracer method is applied. The video records of colored tracers dropped on the spray surface are analyzed by the similar image data processing method to obtain the position in the reference coordinate. The trajectory of the tracer and averaged velocity for a 1/30 second time interval are obtained. Polistyrol tracers about 10*mm* in diameter are chosen after some trials.

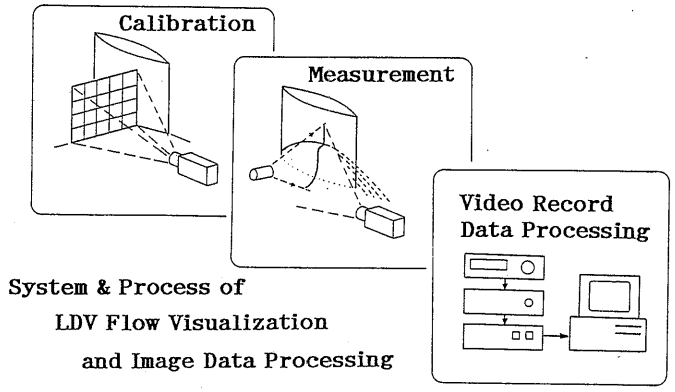

Fig. 3 LASER Flow Visualization and Image Data Processing

2.4 Measurements of Mass Flux and Impulsive Pressure of Spray behind Strut

A simple device shown in Photo 2 and Fig. 4 is applied for the measurement of the spray impulsive pressure. A 50*mm* square flat plate attached to a force gauge is put in the spray. Using this device and a traversing mechanism, a distribution of the spray pressure in the cross section is obtained.

A special device is designed for the measurement of the spray mass flux. It is composed of vertical column with 6 square shaped mouths and a shutter with a time counter, and long vinyl tubes with valves at the other ends. The size and interval of the mouths are 23.4*mm* square and 55.0*mm* respectively. The device for the spray mass flux measurement is shown in Photo 3 and Fig. 5. In the measurement the shutter is opened for few seconds after the carriage reaches a constant speed. The amount of the water in the each tubes are measured by a weight balance after the each run. The mass flux for the position is obtained as the mean value. Considering the unsteady nature of the flow field and the shortage of the duration for the measurements, an ensemble average of the results for several runs is examined and used as the results. As far as the averaged indices and characteristics are concerned, the flow field can be considered almost steady. For the precise investigation, some improvements in the devices and the measurement techniques will be required.

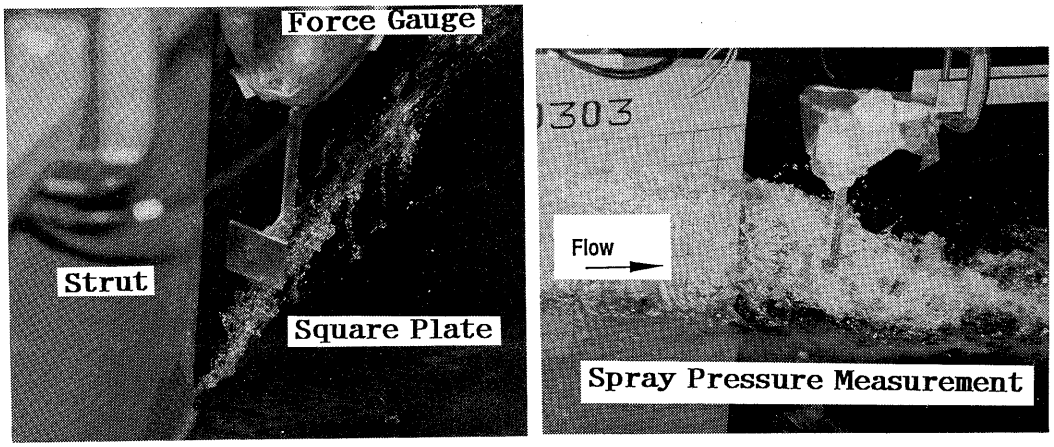

(a) (b)

Photo 2 Device for Measurement of Spray Impulsive Pressure

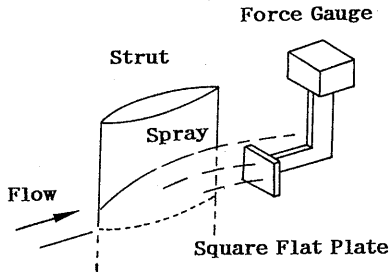

Fig. 4 Device for Measurement of Spray Impulsive Pressure

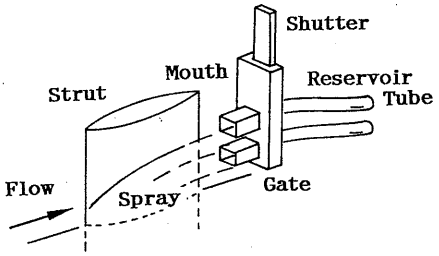

Fig. 5 Device for Measurement of Spray Mass Flux

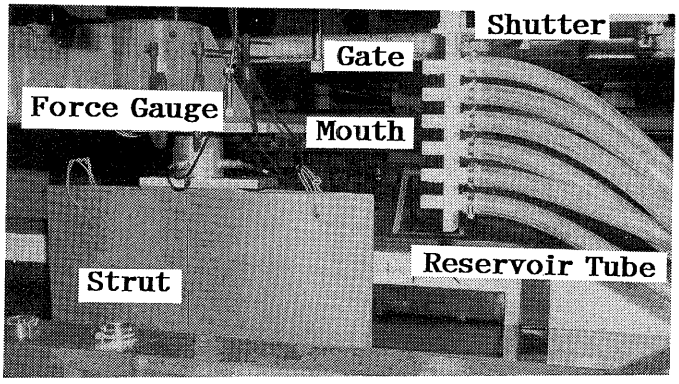

Photo 3 Device for Measurement of Spray Mass Flux

2.5 Turbulence Stimulation and Frictional Drag

Turbulence stimulation by means of trapezoidal studs at bow position (S.S. $9^1/_2$) is used as a standard method in the Ship Research Institute. It is a routine method in the model experiment for conventional and low-speed ships. For the model experiment of high speed crafts, however, any routine method is not established. In the cooperative series test performed in Japan by means of geometrical similar models of semi-planing crafts, knowledge about the scale effects on drag and drag components are obtained. It is reported that the shape and height of the spray are dependent on the size of the ship model [12, 13]. A thorough examination on the similarity law including capillary effects and viscous effects should be performed. In the report of 19th ITTC [8] it is recommended that so-called Hama's Patch is effective and most suitable for the model test of high-speed crafts. Back ground data and investigation of the ITTC recommendation are not clearly shown. In order to improve the accuracy of the prediction of the full scale performance for the *TSL-F* high speed vessel, a fundamental measurement of the various types of turbulence stimulators are carried out. Though the results of the study are not published, it is proved that Hama's Patch and some other stimulators show remarkably better property, i.e. certainty of the stimulation and small inherent drag, than studs, trip wires and sand belts.

Most of the experiments in the present study are carried out without a turbulence stimulator, because they are considered as extensions of the previous work [5] into the higher speed region. As discussed in detail in 3.4, the frictional drag, the majority of the total drag, has a quite sharp sensitivity to the transition and state of the boundary layer. Therefore a stable condition of the boundary layer by the application of the turbulence stimulator is necessary to examine the drag components. A Hama's Patch is applied in a line, $0.04m$ from the leading edge of the larger strut, then the inherent drag of the stimulator is almost compensate to the difference in frictional drag in the region from the leading edge to the stimulator. Measurements of the total drag are performed by changing the total length of the turbulence stimulator. In order to investigate the state of the boundary layer, flow visualization by means of a milk method is applied.

3. RESULTS AND DISCUSSION

3.1 Resistance Test Results and Overall Characteristics of Flow Field

Resistance tests are performed in the speed range Fn=0. 1～3. 0. Neither ventilation nor cavitation is observed.

In Fig. 6 total drag coefficient C_T for various conditions is plotted. They show similar tendency each other for the variation in Froude number except in the dead slow region where some scatter always exist in non-dimensional coefficients. As discussed later in this paper, the difference between the C_T curves of the two models of different size is almost corresponded to the difference in the frictional drag based on the Reynolds number. There are also seen some differences among data for the larger model without turbulent stimulators at the different season, and results with and without the stimulators.

There exist some results of previous studies for the surface-piercing strut with the same or similar cross section [2-4]. The results of Chapman [3,4] increase as the speed increases in the region of Fn=1. 0～2. 0. It is a different trend from the present results. The results of Kaplan [2] show a similar trend to with the present investigation, though there is a

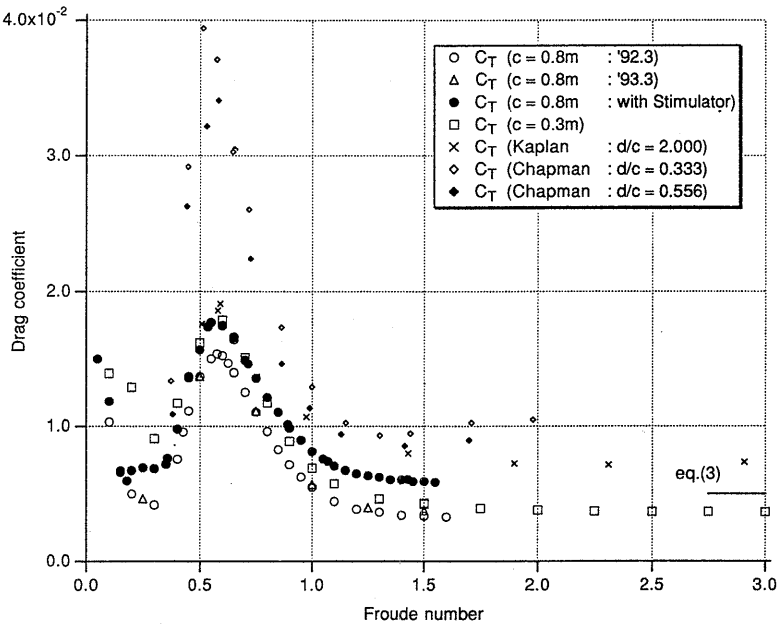

Fig. 6 Results of Resistance Test
(Total Drag Coefficient and Froude Number)

difference in magnitude. The estimated total drag from due to empirical formula given by equation (3) [3] corresponds reasonably to the measured results in Fig. 6.

The flow patterns around the strut are observed. The variation of flow patterns around the same strut for Fn=0.08～1.25 are seen in the report by Takeshi & Adachi [5]. As the speed increases in the slow-speed region, wave-making phenomenon becomes remarkable. The wave-breakings are seen at the crest of waves in the aft part of the model. In the high-speed region Fn>1.1 the massive water elevated above still water level as a wave and a thin water film on the side wall of the strut falls into the water surface after it passes the aft end where a smooth water surface no longer exists. This is considered as the essential part of the spray.

The flow field around the strut at Fn=1.5 is intensively examined by the flow measurements. The wave elevation and the shape of the spray envelope are measured and compared with a CFD simulation solving an Euler equations [14]. In Fig. 7 a bird's-eye view of the calculated wave pattern around the strut at Fn=1.5 is shown. Except the spray and wave-breaking, the whole pattern seems to be quite realistic. As seen in Figs. 8～10 results of measurement and calculation show a good agreement for the wave elevation in Fn=1.5 except on the wall of the strut and near field region behind the strut. The former disagreement stems from the grid size in the calculation and the latter from the water fall of the spray [14].

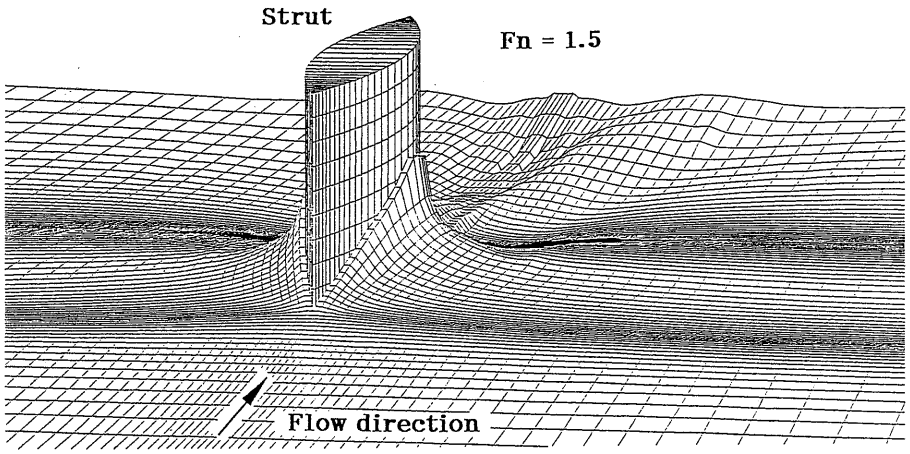

Fig. 7 Bird's-eye View of Calculated Waves

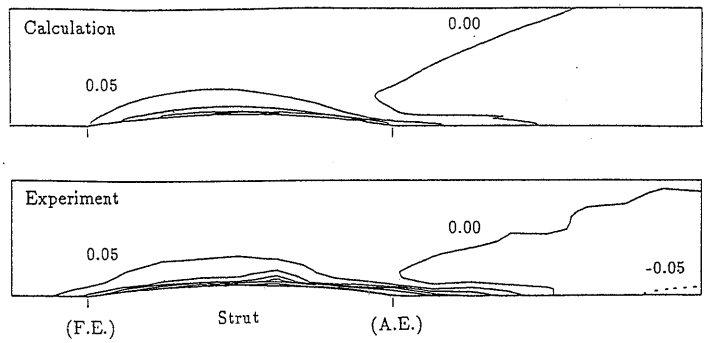

Fig. 8 Comparison of Measured and Calculated Wave Contours (Fn=1.5) (Contour interval is 0.05 × c, Dotted lines show negative value)

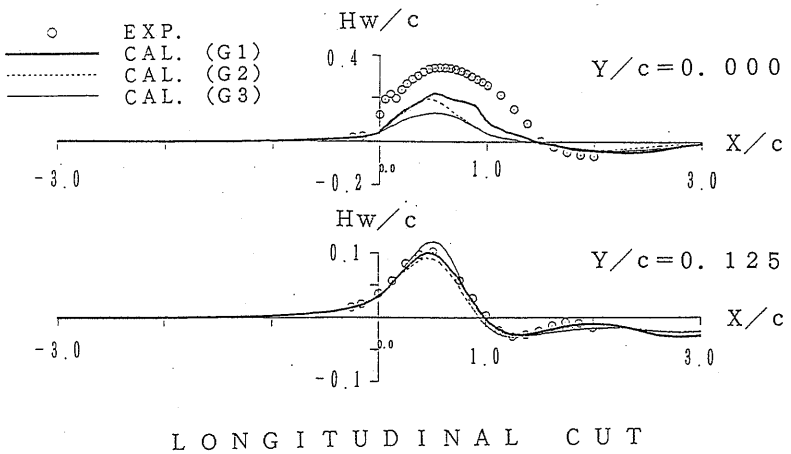

Fig. 9 Comparison of Measured and Calculated Longitudinal Wave Profiles (Fn=1.5)

The wetted surface area is important in practice and it is obtained by an oil paint method and the analysis of photographic and video records. Photo 4 shows a result of the oil paint test at Fn=1.5. In the high speed region, the wetted area increases monotonously as the speed increases. The wave profiles on the side wall of the strut for several Froude number are shown in a previous study [5], and the results in Fig. 9 for Fn=1.5 are an extension into the higher speed region.

Measurements on the larger strut are repeated several times. Some

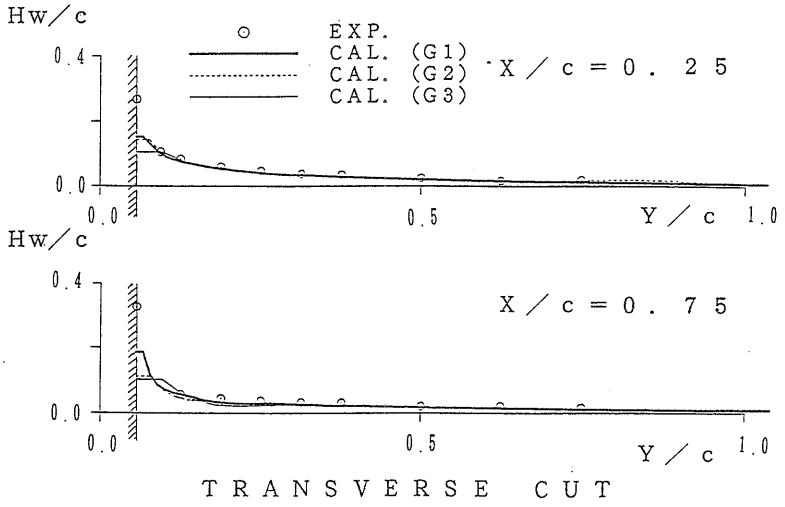

Fig. 10 Comparison of Measured and Calculated Wave Profiles at a given Cross Section (Fn=1.5)

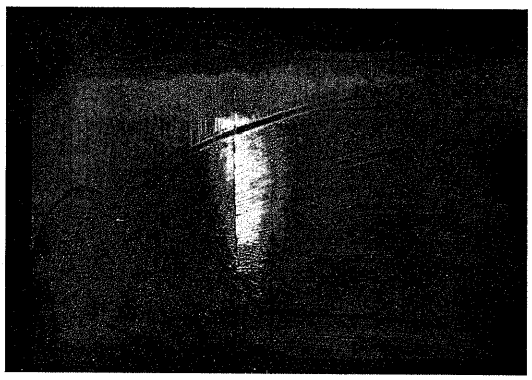

Photo 4 Result of Oil Paint Test (Fn=1.5)

discrepancies are seen in the measurement for the same condition. There are two possible causes for the discrepancis and uncertainty in the repeatability. One is due to the model condition, i.e. a deformation of the model, minor difference in the shape due to the surface treatment. And the other is changes of the conditions in the measurement i.e. accuracy of setting of the force gauge and the model etc. Therefore it is not suitable to discuss on the flow structure and drag in too much detail. The repeatability of the results, however, is satisfactorily on the whole. The difference in the drag for larger and smaller models, and with and without a turbulence stimulator seems to be significant and is discussed later in this paper.

3.2 Spray Shape and Velocity

Photo 5 shows the spray at Fn=1.5 from various view points. Photo 5 (e) & (f) show the spray from the strut with Hama's Patch. There are two parabolic envelopes of the spray seen on the side wall of the strut. The first initiates from a wave-breaking observed at 6% chord position and the spray falls in the water surface near the mid-chord . The second is from the position of 12.5% chord position, reaches a peak at 60% chord, and falls about 30~50% of chord length behind the aft end of the strut. The spray separates at all the position along the upper envelope of the wave and the clusters of water drops fly into the air and fall to the water surface. The water surface creeps up along the side wall of the strut and a thin film of water is formed. The thin film either separates and breaks into water droplets, or the thin film breaks into *bore-like* waves, breaking at the wave crest and water drops are formed. Obviously the spray is not a steady phenomenon. In Figs. 11~13 the shapes of the spray visualized by LASER technique are shown [11].

The trajectory and velocity on the spray are measured by means of a similar image data processing technique applied to the video records of the tracers on the spray. In Fig. 14 the measured velocity vectors are shown at Fn=1.5 condition. According to an inviscid discontinuous flow model, where a hodograph method and a conformal transformation are applied in the 2-dimensional flow, the velocity on the spray coincides to the free stream velocity which is equal to the advancing speed. It is seen, however, that the measured velocity is smaller than the advancing speed. Similar results were shown for the spray of planing boats and seaplanes [9, 10].

Once water particles separate from the water surface and fly into the air, a quite simple mechanism of the dynamics will govern the flow in stead of the governing equations for a continuum in the hydrodynamics. The following free fall model is applied to the spray.

$$m\frac{d^2\boldsymbol{r}}{dt^2} = -mg\boldsymbol{e}_z - \alpha\frac{d\boldsymbol{r}}{dt} \tag{1}$$

Because air drag has a less important effect on the final solution than the initial velocity, the air drag term in the model is neglected. ($\alpha \to 0$) Taking a new coordinate system xyz such that the *xz-plane* is coincident to the initial velocity direction and giving an initial position (X_0, Y_0, Z_0) and a

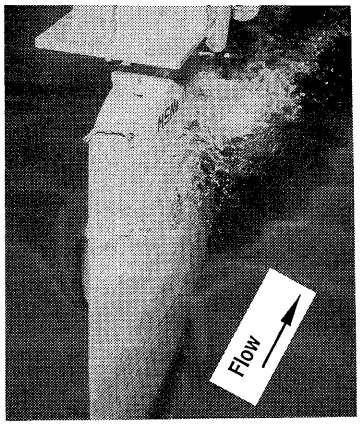

(a)

(b)

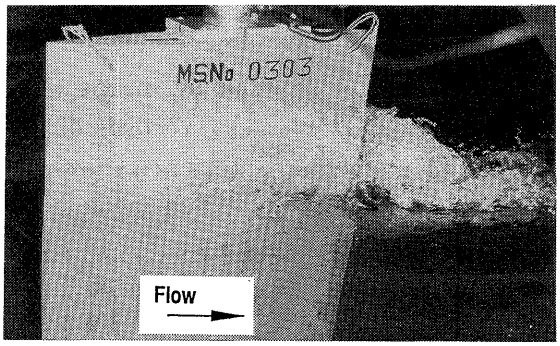

(c)

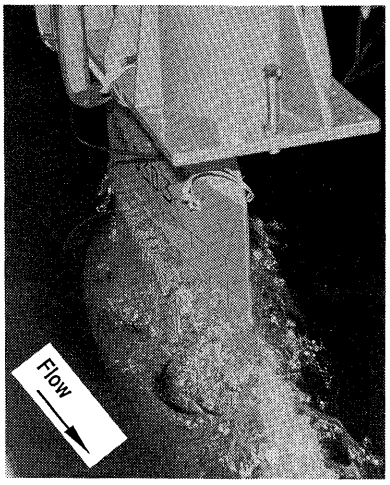

(d)

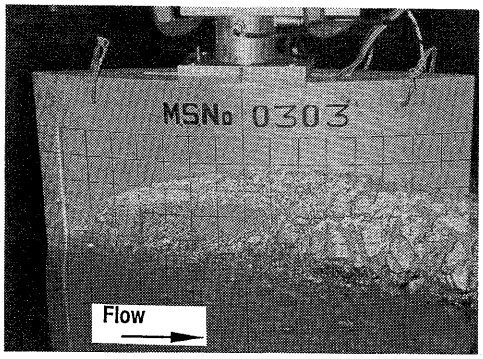

(e)

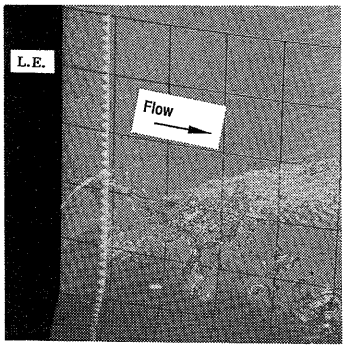

(f)

Photo 5 Spray from Surface-Piercing Strut (Fn=1.5)

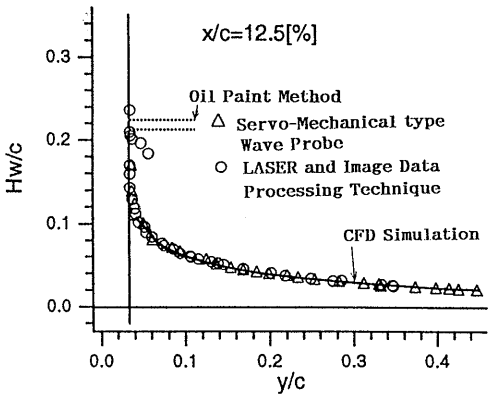

Fig. 11 Typical Spray Shape and Wave Elevation in a Cross Section (Forebody, Fn=1.5)

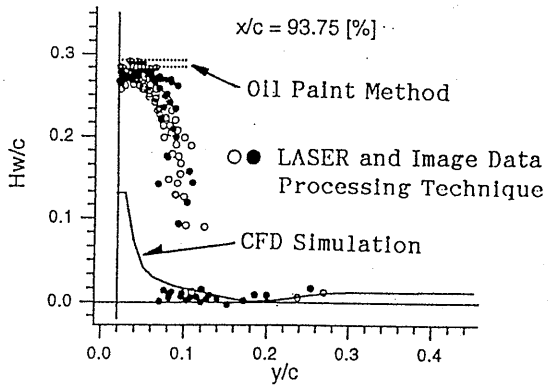

Fig. 12 Typical Spray Shape and Wave Elevation in a Cross Section (Aftbody, Fn=1.5)

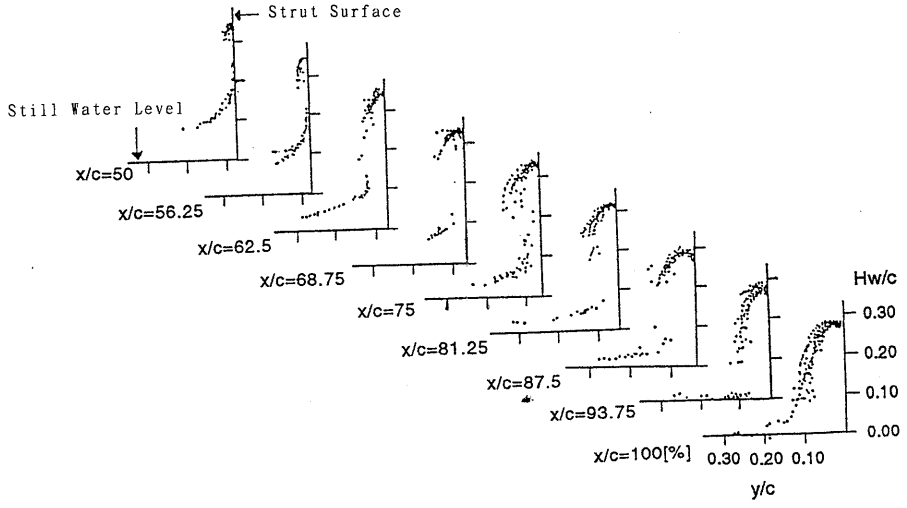

Fig. 13 Longitudinal Variation of Spray visualized by LASER Sheet (Fn=1.5)

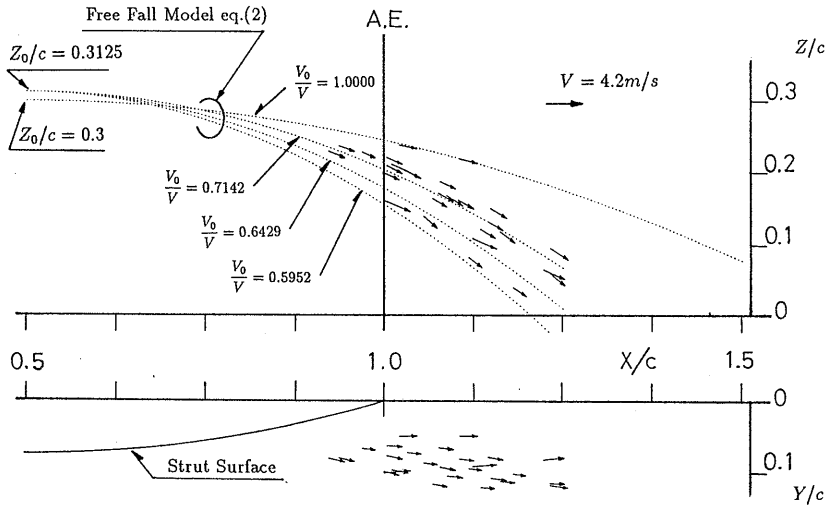

Fig. 14 Velocity Vectors on Spray Surface (Fn=1.5)

velocity V_0, the trajectory of the particle is in the Y=Y_0 plane is given as;

$$\frac{Z}{c}-\frac{Z_0}{c}\sim-\frac{1}{2F_{n0}^{\,2}}\cdot\left(\frac{X}{c}-\frac{X_0}{c}\right)^2 \qquad as \quad \alpha\to 0 \tag{2}$$

$$where \qquad F_{n0}=\frac{V_0}{\sqrt{gc}}$$

According to the model, the nature and structure of the spray are investigated and compared to some measured results as follows. The initial position of the spray is clearly determined by the measurement, but the initial velocity is unknown and difficult to be measured accurately. By means of the identification techniques the unknown initial velocity is determined so as to explain the measured position, shape and/or trajectories of the spray. In Fig. 14 the identified trajectories projected on the center plane of the strut are shown as dotted lines. It is seen that the measured trajectories fit equation (2) well, and the identified initial velocity of the spray V_0 shows reasonable agreement with that obtained by the tracer method. These velocities are 70~80% of the advancing speed.

In the plan view it is seen that some of the trajectories drawn by the velocity vectors do not remain in the original plane. Of course it is difficult to explain this fact by the simple free fall model. Possible reasons of the curve are an interaction with other water particles and an influence of the air flow along the strut curvature.

3.3 Mass and Momentum Flux of Spray

Fig. 15 shows the mass flux distribution in a cross section and the lateral distribution of the accumulation of flux. The latter curve is obtained by the integration along the vertical line for the region from Z/c=0. 0281 to 0. 281. It is difficult to distinguish the boarder of the spray and the wave surface near the still water level, because neither conventional wave sensors nor the configuration of the flow visualization mentioned before are available there. For the analysis of the momentum loss, the boarder is assumed at Z/c=0. 0281 position where the measured results show drastic changes. The assumed boarder is proved to be acceptable by later measurement. The successful measurement of the wave surface behind the strut in the spray region is by means of a water proof video camera from the bottom position of the strut, though further examinations of the accuracy and precise calibration are necessary. As shown in Fig. 16, similar patterns are obtained for the measured contour of impulsive spray pressure and the lateral distribution of its accumulation. The difference between the patterns of the spray mass flux and impulsive pressure seen in the lower part of the cross section originates from the difference in the contribution of the average velocity on flux and momentum. Of course the difference of the segment sizes in the measurements is considered as an another possible reason. In order to draw fine contour curves, a smaller

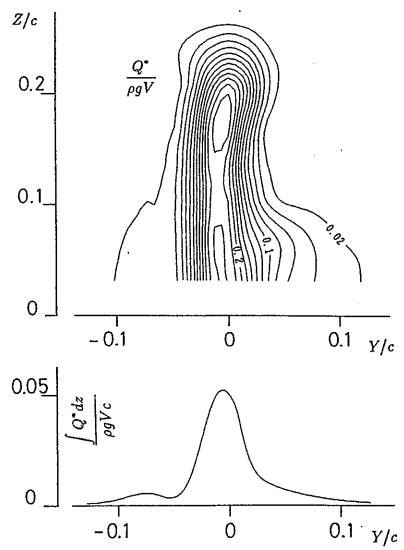

Fig. 15 Measured Mass Flux Distribution (Fn=1.5, X/c=112.5%)

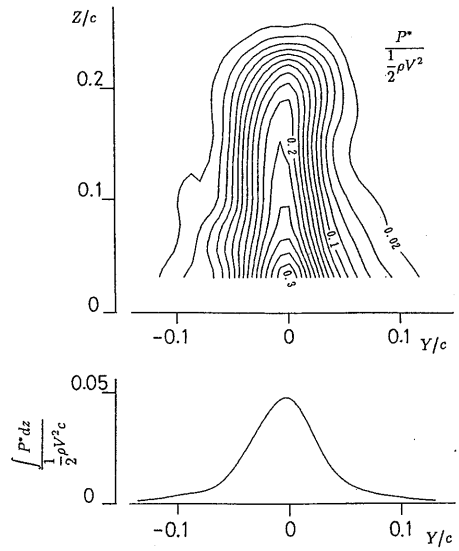

Fig. 16 Measured Impulsive Pressure Distribution (Fn=1.5, X/c=112.5%)

flat plate and square mouths, and/or fine mesh measurement are required. On the other hand an improvement in the accuracy of the total impulsive pressure and mass flux will be brought about by bigger sizes of the mouth and flat plate. From Figs. 15 & 16 it is seen that the distribution of mass and momentum flux concentrate in the relatively narrow region near the center plane of the strut, though the spray spreads over a wider range behind the strut.

Using the measured results for the mass flux and impulsive pressure of the spray, the average value of the stream velocity and the momentum of the flow are obtained. The mean velocity almost correspondes to that measured by the tracer method.

3.4 Drag Components [15]

3.4.1 Separation of drag components

There are several ways of separating and expressing the drag components. Among them there are two categories. The first is a separation according to the portions of body. This is quite simple and frequently used in practice. For example in aircraft design the total drag is composed of drags of wing, fuselage and tails etc.. Once a comprehensive data basis is established, this method of estimation becomes a quite powerful tool for a practical design. The following is an empirical non-dimensional formula for a strut proposed by Chapman [3], for the higher speed region $Fn \geqq 3$.

$$C_T \sim C_{PROFILE} + C_{SPRAY} + C_{TIP} \tag{3}$$

The total drag is composed of profile drag, spray drag and tip drag.

There are different formula available in the lower speed region in which a wave-making drag by means of the thin ship theory is taken into account. [3]

The tip drag represents the 3-dimensional effect of the flow, and the spray drag including wave-making drag is due to the free surface effect. They are expressed as functions of thickness ratio and draft ratio. For the double arc strut they are given as:

$$C_{SPRAY} \sim 0.011\left(\frac{B}{2d}\right) + 0.08\left(\frac{B}{c}\right)\left(\frac{B}{2d}\right) \tag{4}$$

$$C_{TIP} \sim -0.02\left(\frac{B}{c}\right)\left(\frac{B}{2d}\right) \tag{5}$$

The profile drag expressed by " section drag" [3] acts on the middle part of the strut, the tip drag on the bottom part, and the spray on the above water part of the strut. Therefore the empirical formula can be considered as an example of the first category.

The profile drag of the strut obtained in the previous study [5] is shown as follows:

$$C_{PROFILE} \sim 0.4 \times 10^{-2} \tag{6}$$

The estimated total drag calculated by equation (3) with the profile drag is shown in Fig. 6.

The other category of drag component separation is based on the hydrodynamic mechanism of the drag and the flow field. Because some factors of different nature govern a flow field with free water surfaces, this kind of method offers a rational basis for the estimation of a full scale performance through model experiments. For example, wave making drag depends on the Froude number, viscous and frictional drag on the Reynolds number, spray drag on the Weber number etc.. In order to simplify the present investigation, the following form is assumed.

$$C_T = C_V + C_W + C_{SPRAY} + C_{RES} \tag{7}$$

$$C_V = C_{F0}(1+k) \tag{8}$$

where C_{RES} is the generalized residuary drag coefficient. The viscous drag is expressed as equation (8) using the frictional drag and form factor. The residuary drag contains interaction effects of drag components and components due to other negligible flow mechanisms. The other two components are specific to flow with a free water surface. Assuming the residuary drag to be zero in the first order approximation, we have;

$$C_T = C_{F0}(1+k) + C_W + C_{SPRAY} \tag{9}$$

3.4.2 Wave-making drag and viscous drag

In Fig. 17 the wave-making drag by the thin ship theory, C_W, and calculated curves of the frictional drag for the equivalent flat plate, C_{F0}, are shown with the measured total drag coefficients, C_T.

Though there are some uncertain factors, the contribution of each component to the total drag in each speed region is demonstrated in the

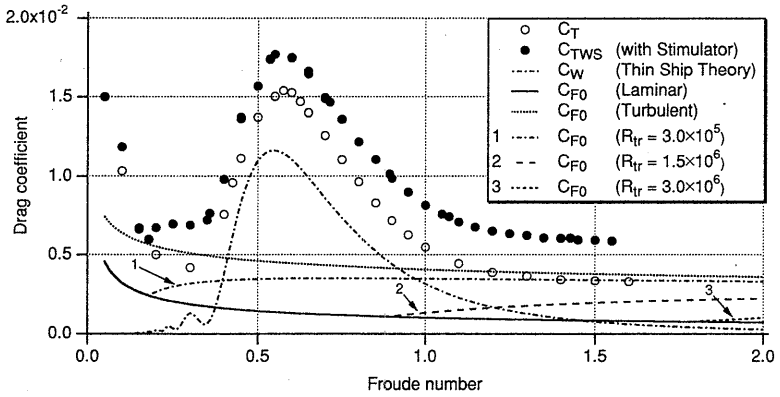

Fig. 17 Wave-Making Drag by Thin Ship Theory and Frictional Drag

figure. The choice of formula for the frictional drag, and the estimation of the transition position and the form factor are the uncertainties in practice.

So long as waves in the far field and the variation of the wave-making drag in Froude number are concerned, the thin ship theory gives a sufficient guideline in practice. Other analytical methods of wave-making theory available for the whole region have already been applied and examined [5]. If necessary, CFD techniques are also available for more general problems. Therefore it is concluded that the theoretical estimations for wave-making problems are well established.

Viscous drag is estimated by the theoretical and empirical formula for an equivalent flat plate and a form factor. With regards to the boundary layer transition, the frictional drag coefficient C_{F0}, is given as a function of Reynolds number.

$$C_{F0}(R_n)=\begin{cases} C_{F0}(R_n)|_{\mathrm{lam}} & R_n \le R_{tr} \\ C_{F0}(R_n)|_{\mathrm{turb}}-\dfrac{R_{tr}}{R_n}\{C_{F0}(R_{tr})|_{\mathrm{turb}}-C_{F0}(R_{tr})|_{\mathrm{lam}}\} & \text{otherwise} \end{cases} \tag{10}$$

where R_n and R_{tr} are Reynolds numbers for the measurement and transition respectively.

The three curves corresponding to the different assumptions of the transition Reynolds number R_{tr} are shown in Fig. 17 with the curves for fully turbulent and laminar boundary layer. The upper and lower transition Reynolds number $R_{tr}=3\times10^6$ and $R_{tr}=3\times10^5$ are the values shown in the experimental studies on a flat plate. Provided these results are applicable to the strut, these two curves define a possible band for the

frictional drag of the strut without the turbulence stimulators. The intermediate curve corresponds to the transition Reynolds number $R_{tr}=1.5\times10^6$ obtained in the present study shown in section 3.4.3. The curve for the full turbulence state corresponds to the condition with the turbulent stimulators.

As seen in Fig. 17 there is a considerably wide band of value for the frictional drag unless the state of the boundary layer is known. Therefore it is possible to explain the discrepancies between the total drag among different experiments mentioned in section 3.1 as the differences in the frictional drag due to the boundary layer condition. The difference between the drag in the present experiment and Kaplan's experiments performed with the turbulence stimulator is almost comparative to the difference between turbulent and laminar flow. It seems reasonable that the frictional component rather than the spray is the cause of the discrepancy. The different tendency obtained by Chapman for Fn=1.0～2.0 may be explained as the transition of the boundary layer. Considering these conditions, the drag curves in Fig. 6 and equation (9) together, it is predicted that most of the boundary layer on the strut without turbulence stimulators remains in a laminar state.

In Fig. 18 the same measured data of the total drag are plotted against Reynolds number. From the figure the contribution of the frictional drag to the differences of the total drag between the larger and smaller models, and with and without turbulence stimulator are more clearly seen. In principle, it is also possible to determine the form factor from the results of the geometrically similar models of different sizes. Applying the method

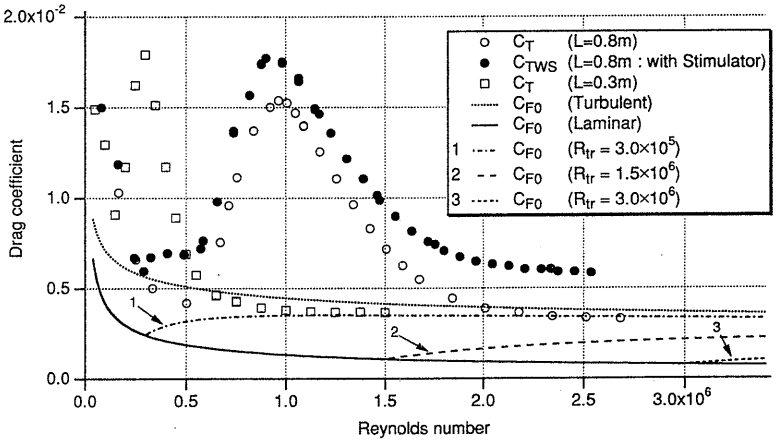

Fig. 18 Total Drag and Frictional Drag against Reynolds Number

to the present results in relatively high speed region, where S/N ratio of the measurement is good, the form factor obtained shows a large band of estimation k=−0.6∼2.5. Obviously the transition of the boundary layer is one of the reasons for the wide band, because reference data are for the strut without a turbulence stimulator. In order to determine the form factor, careful measurements in the condition with turbulence stimulators are required.

As a theoretical method for the viscous drag estimation, the solution of the boundary layer equation and CFD calculation of Navier-Stokes equations are representative. But both are not well evaluated in practice.

3.4.3 Estimation of state of boundary layer and turbulence stimulator

Photo 6 shows examples of the results of flow visualization by means of a milk method. It is seen from the results that the flow in the boundary layer leeward of the Hama's patch is turbulent. It is also clear that the boundary layer remains laminar for more than half the chord without the turbulence stimulator in the lower speed region. But the milk method does not seem to be valid in the higher speed region. Because the milk diffuses within a far shorter distance than predicted by the results of the total drag measurement with and without turbulence stimulator.

The difference in the total drag due to the length of turbulence stimulator are examined. As seen in Fig. 19, the measured results of total drag vary linearly according to the length of the turbulence stimulator

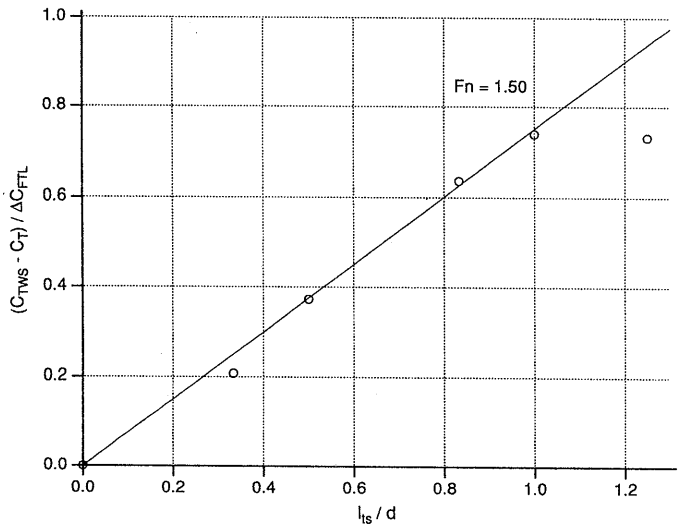

Fig. 19 Effect of Length of Turbulence Stimulator on Total Drag

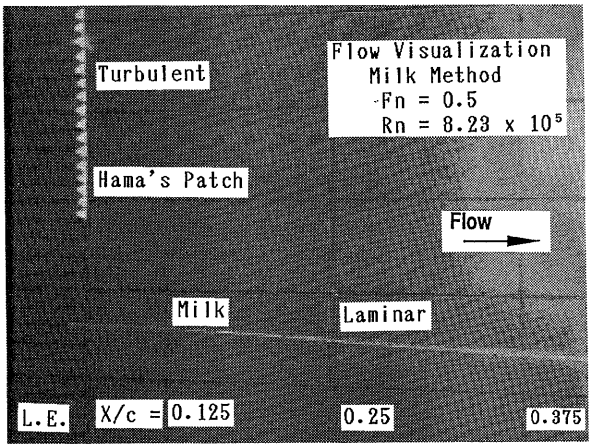

(a)

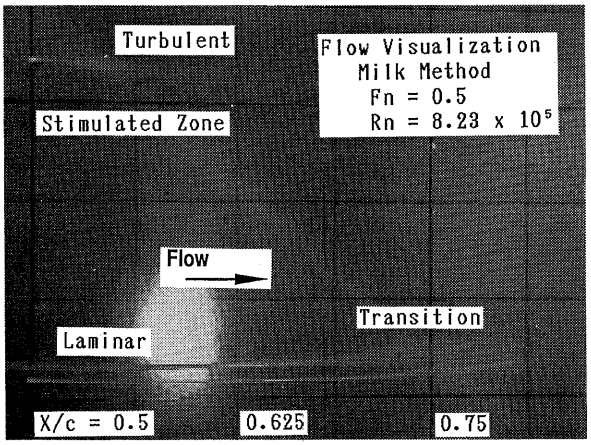

(b)

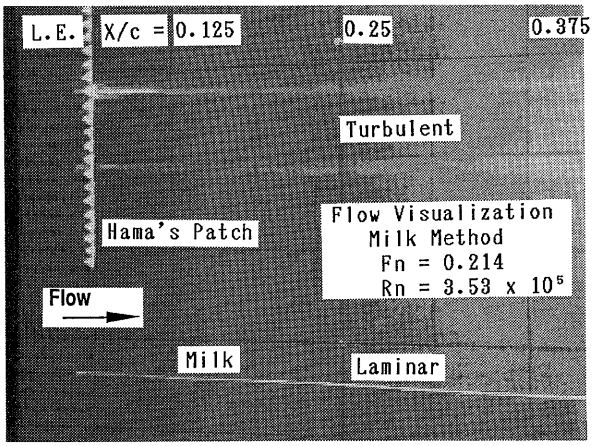

(c)

Photo 6 Results of Flow Visualization by Milk Method

except a plot in $l_{ts}/d>1$. Difference of the drag with and without the turbulence stimulator is smaller than the difference of frictional drags between entirely laminar and fully turbulent states. Provided the state of the boundary layer is fully turbulent by means of the turbulence stimulator on the full of the strut depth, it is concluded that the state corresponding to the condition without turbulence stimulator is not fully laminar. On the assumption of the frictional drag obtained by the ratio of the area of laminar and a turbulent states, it is possible to derive the transition position in the boundary layer. Provided the form factor $k=0.1\sim0.3$ at $Fn=1.5$, it is founded that the transition of the boundary layer occurs at about $0.5m$ from the leading edge of the strut, i.e. the transition Reynolds number $R_{tr}=1.5\times10^6$. The result almost corresponds to that obtained by 2-dimensional boundary layer equation of integrated type [5].

3.4.4 Spray drag

The spray drag is defined by the momentum loss as;

$$D_{SPRAY}=Vm^*-P^*=V\frac{Q^*}{g}-P^* \tag{11}$$

$$C_{SPRAY}=\frac{D_{SPRAY}}{\frac{1}{2}\rho V^2 S}=\frac{2\left(\frac{Q^*}{\rho g V}\right)-\left(\frac{P^*}{\frac{1}{2}\rho V^2}\right)}{S} \tag{12}$$

where m^*, P^* and Q^* are mass flux rate, impulsive pressure of the total

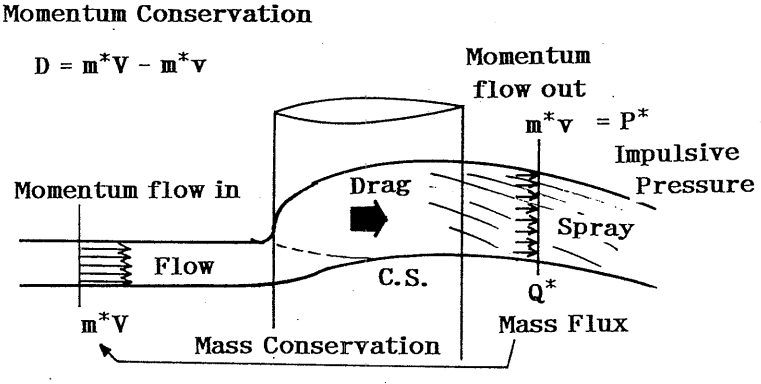

Fig. 20 Control Surface for Spray Momentum Investigation

spray and flux rate of water in weight respectively. Taking control surfaces shown in Fig. 20 for the momentum investigation, the spray drag coefficient C_{SPRAY} estimated by the measurement of the spray flux and impulsive pressure can be obtained. Let the control surface in the upstream direction be far enough from the strut so that the velocity equal is to the uniform velocity V, the inflow momentum flux across the control surface is m^*V. The mass flux m^* is equal to that at the control surface behind the strut because of the mass conservation law. Applying the conservation law for momentum over the whole of the control surface, the spray drag defined as the momentum loss in x-component is obtained as equation (11).

3.4.5 Total drag and drag composition

The estimated drag components of the strut with and without the turbulence stimulators for Fn=1.5 are shown as bar graphs in Figs. 21 & 22 respectively. The measured total drag coefficient is compared with the estimated values from equation (9). Uncertainty ranges of each component are shown as arrows in Fig. 21.

It is seen that the average value gives a reasonable estimate, though it contains a large amount of uncertainty.

The arrow mark for the total drag, which is determined by the scatter found in the measurements, corresponds to the uncertainty due to the accuracy and the repeatability discussed in section 3.1. The uncertainty of the viscous drag comes from the frictional drag C_{F0}, and form factor k. The longer arrows for the total and viscous drag in Fig. 21 correspond to the results including both effects and the shorter only the form factor. Therefore the range without turbulence stimulator shown in Fig. 21 has a wider band than that for with the turbulent stimulator in Fig. 22. When the most suitable frictional drag coefficient is chosen, there are still two alternatives due to the wetted surface area. The first is the area for the still water condition and another is the area for the experimental condition. For evaluation of the viscous or frictional components themselves the latter is reasonable. On the other hand the former is better for the estimation of the total drag, because some part of the frictional drag increase due to the swell on the side wall which will be counted as a momentum loss measured in the spray drag.

For the estimation of the wave making drag, C_{WP}, wave pattern analysis of the measured wave is used. The uncertainty range is due to the

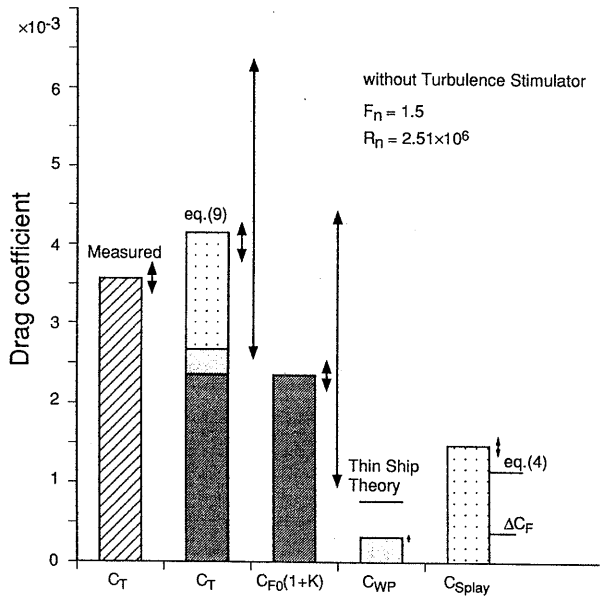

Fig. 21 Estimated Drag Components of Strut without Turbulence Stimulator

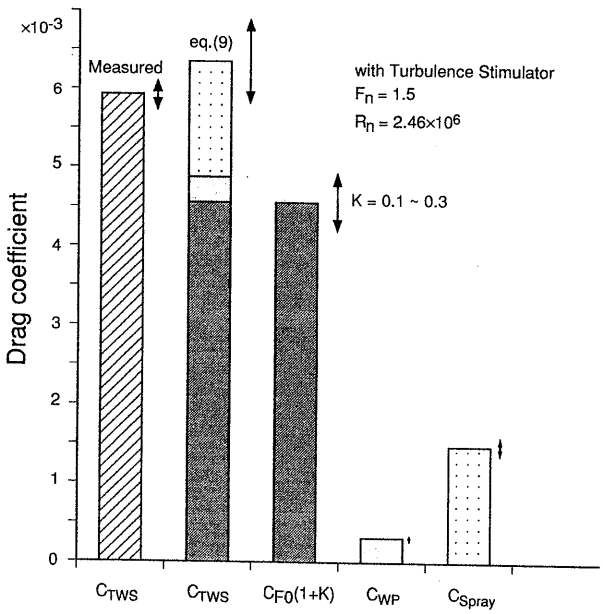

Fig. 22 Estimated Drag Components of Strut with Turbulence Stimulator

dependency of the results on the longitudinal cut position [5]. So long as a linear water wave theory is based and the position of the wave measurement is far from the strut, the dependency will not appear. Therefore the uncertainty range comes from the nonlinear behavior of the surface waves. Another kind of wave-making drag is calculated by the thin ship theory. As seen in Fig. 21 the measured value C_{WP}, is smaller than the calculated C_W. Provided C_W represent the drag due to the wave-making by the advancing strut and C_{WP} corresponds to the energy propagation by wave motion, the latter should be smaller than the former. For the lower speed region discussed in the previous work [5] the difference is explained as the transformation of the wave energy into the viscous wake by wave-breaking phenomena. In the present case it is assumed that the difference is caused by the energy transfer to the spray.

The spray drag obtained by the momentum loss is also shown in Fig. 21. The uncertainty range comes from the arbitrary range of integration and the accuracy of the measurement. It is concluded said that the frictional drag due to the wetted surface by the spray is a considerable part of spray drag. [3] Sometimes this component ΔC_F represents the spray drag in practice. As seen in Fig. 21 ΔC_F is smaller than C_{SPRAY} in the present case. This is reasonable because the skin friction is one of the causes of momentum loss. The estimated value of C_{SPRAY} due to Chapman's empirical formula (4) is shown in Fig. 21. They show reasonable correspondence to the present results.

In Fig. 22, bar graphs of drag components of the strut for the condition with a turbulence stimulator are shown. The uncertainty range of the total drag coefficient C_T, due to the scatter of data is used in case that the strut without turbulence stimulator is measured. The viscous drag is estimated for the fully turbulent state. The uncertainty range for the viscous drag C_V, comes from the form factor k. Spray drag and wave-making drag measured by the strut without a turbulence stimulator is used. Considering the uncertainty, it is said that the agreement of the measured and estimated C_T is quite satisfactory. The uncertainty range becomes narrower with the turbulence stimulators. This is quite important in practice, because the usual objective of the model experiment is to have an accurate estimation of the full scale performance. Turbulence stimulation by Hama's Patch is quite useful for high speed model test.

4. CONCLUSIONS

Through the experimental study on the spray separated from a strut model, the following conclusions are obtained.

1) In the speed region $Fn>1.1$, the water elevated along the strut flies into the air as a spray from the aft end of the strut. The spray also initiates along the envelope of the elevated waves on the side wall. The spray becomes stronger as the speed increases. Except wave-breakings and the spray, the measured wave pattern around the strut is quite similar to that of the calculated results for the inviscid flow by a CFD technique.
2) The shape of the spray is measured by means of the flow visualization and image data processing technique. The spray shows parabolic trajectory. A free fall model is applied to the analysis of the trajectories obtained by a tracer method. It is seen that the free fall model, neglecting air drag, gives good estimate as the first approximation. The initial velocity of the water particles in the spray identified by the model are 70~80% of the advancing speed.
3) The spray drag due to the momentum loss is estimated by the measurement of the spray mass flux and impulsive pressure behind the aft end.
4) The drag components at $Fn=1.5$ are examined, and it is seen that the major component is the frictional drag, followed by the spray drag. The wave-making drag is not so large in the given condition. Hama's Patch is shown to be effective as a turbulence stimulator for high speed experiments.

Acknowledgement

The authors would like to acknowledge the continuing guidance and encouragement of Dr. H. Kitagawa, the Directer-General of the Ship Research Institute. The authors also wish to express their thanks to Mr. H. Takeshi and their colleagues in the the Ship Performance Division for their valuable discussions and helpful advices.

References

1) Fuwa, T., Hirata, N., Hori, T. & Fujisawa, J. : Experimental Study on Spray Separated from an Advancing Surface-Piercing Strut at High

Speed, 2nd International Conference for High Performance Vehicle (HPV'92-CHINA), Shenzhen, 1992.

2) Kaplan, P. : Tests of Surface-Piercing Struts, Stevens Institute of Technology, Stevens ETT Report 488, 1953.

3) Chapman, R.B. : Spray Drag of Surface-Piercing Struts, AIAA/ SNAME/USN Advanced Marine Vehicles Meeting, 1972.

4) Chapman,R.B.: Hydrodynamic Drag Measurements on SWATH Ship Components,Naval Undersea Center NUC TP 406, 1974.

5) Takeshi,H. & Adachi,H: On the Separation of Resistance Components of Surface-piercing Strut at Large Froude Numbers, Report of Ship Research Institute Vol.18, No.3, May 1981. (in Japanese)

6) Muller-Graf,B.: The Effect of an Advanced Spray Rail System on Resistance and Development of Spray of Semi-Displacement Round Bilge Hulls, FAST'91, Trondheim, 1991.

7) Bjorklund, J.Hellstrom, S.: Spray Rails on Planing Vessels Model Tests and Experience from Built Boats,International Symposium on Ship and Shipping Research, 1992.

8) Proceedings, High-Speed Marine Vehicle Committee, 19th ITTC, 1990.

9) Hirano, S., Inatsu, S. & Himeno, Y. : Observation of the Spray of Prismatic Planing-Hull Models, Journal of the KANSAI Society of Naval Architects, JAPAN, No.217, 1990. (in Japanese)

10) Kikuhara, S. : A Study of Spray Generated by Seaplane Hulls, Journal of the Aero/Space Sciences, Vol.27, No.6, 1960.

11) Fujisawa, J. and others : Spray of Surface-Piercing Strut at High Speed, 60th General Meeting of Ship Research Institute, 1992. (in Japanese)

12) Tanaka, H. and others : Cooperative Resistance Tests with Geosim Models of a High-Speed Semi-Displacement Craft, Journal of Society of Naval Architects of Japan, Vol.169, 1991.

13) Ueda, T., Tsukada, Y. & Sugai, N. : Some Consideration on Tank Test and Power Estimation of Semi-Displacement Type Mono-Hull Ship, Report of Ship Research Institute, Vol.29, No.2, 1992. (in Japanese)

14) Hirata, N. and others : Flow Field around a Vertical Strut at High Speed, 56th Annual Meeting of Ship Research Institute,1990. (in Japanese)

15) Fujisawa, J., Hori, T. & Hirata, N. : On spray drag of an advancing surface-piercing strut at high-speed, 42th Japan National Congress of Theoretical and Applied Mechanics, Tokyo, 1993. (in Japanese)